PCCP

Accepted Manuscript

ROYAL SOCIETY OF CHEMISTRY

www.rsc.org/pccp

Graphic abstract

A ferromagnetic nanocrystallines containing copper as an efficient catalyst for photoinduced water oxidation

Xiaoqiang Du[a] , Yong Ding[*a,b], Rui Xiang [a], Xu Xiang [b]

[a] State Key Laboratory of Applied Organic Chemistry and College of Chemistry and Chemical Engineering, Lanzhou University, Lanzhou 730000, China

[b] State Key Laboratory of Chemical Resource Engineering, Beijing University of Chemical Technology

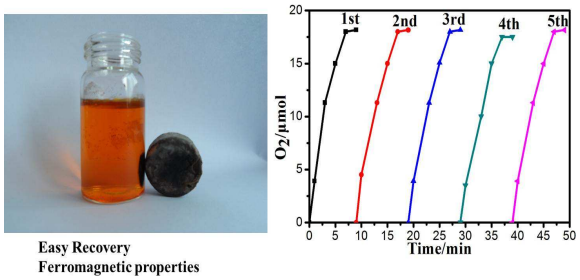

$CuFe_2O_4$ nanocrystallines with cubic jacobsite structure showed remarkable photocatalytic water oxidation activity with an apparent TOF value of 1.2 $\mu mols^{-1}m^{-2}$.

Journal Name

RSCPublishing

ARTICLE

A ferromagnetic nanocrystallines containing copper as an efficient catalyst for photoinduced water oxidation

Cite this: DOI: 10.1039/x0xx00000x

Received 00th January 2012,
Accepted 00th January 2012

DOI: 10.1039/x0xx00000x

www.rsc.org/

Xiaoqiang Du[a] , Yong Ding[*a,b], Rui Xiang [a], Xu Xiang [b]

$CuFe_2O_4$ nanocrystallines with cubic jacobsite structure have been obtained by heat treatment of coprecipitation product, which were synthesized by reaction of Cu^{2+} ions and Fe^{3+} ions in alkaline condition. Reported here is the first copper-based catalyst in photocatalytic water oxidation using $[Ru(bpy)_3]Cl_2$ as the photosensitizer and $Na_2S_2O_8$ as the sacrificial electron acceptor, respectively. An apparent TOF value of 1.2 $\mu mols^{-1}m^{-2}$ and oxygen yield of 72.8% were obtained with $CuFe_2O_4$. The apparent TOF value with $CuFe_2O_4$ (1.2 $\mu mols^{-1}m^{-2}$) is the highest value among all heterogeneous photocatalytic water oxidation systems. The $CuFe_2O_4$ can be easily separated from reaction solution by magnetic separation while maintaining excellent water oxidation activity in the fourth and fifth runs. The surface conditions of $CuFe_2O_4$ is slightly absence after examination by X-ray photoelectron spectroscopy (XPS) before and after the photocatalytic reaction.

Introduction

Artificial photosynthetic solar fuel production that directly converts solar energy into chemical energy is so far considered to be an promising system for the generation of hydrocarbon fuels using solar energy[1]. Nature's cuboidal $CaMn_4O_5$ oxygen evolving complex (OEC) of photosystem II (PSII) is the key paradigm for biomimetic water oxidation catalyst (WOC) design. To date, however, the synthesis of high performance Mn-cubane water oxidation catalysts still remains challenging, and the number of known Co_4O_4-based WOCs is limited to selected Co(II)-containing representatives [2]. Moreover, Fe_4O_4 -based WOCs have not yet to be reported in the photocatalytic water oxidation.

Noble metals such as iridium[3-5] and ruthenium[6-9] were previously reported to act as efficient catalysts for water oxidation. However, in order to be economically viable, some other first-row transition metals[10-15] are more promising WOCs owing to their less expensive, environmentally benign, and relatively nontoxic properties. Various materials have been studied for water oxidation, such as metal complexes with organic ligands[16-23], polyoxometalates[24-29] and simple salts[30]. Recently, first-row transition metal oxide materials have attracted much attention as potential materials for water oxidation, since they are inexpensive, non-toxic and earth-abundant materials. To improve the catalytic activity of oxide materials, various methods have been studied. For example, doping with trivalent metal ions such as La^{3+} has been reported to improve the catalytic activity of cobalt oxides for photocatalytic water oxidation[31]. Moreover, Fukuzumi et al[32] reported a highly active and robust catalyst composed of iron-based oxide doped with foreign elements (M=Ni^{2+}, Mg^{2+} or Mn^{2+}) for the photocatalytic water oxidation. However, doping of foreign metal ions to copper oxides which are much more earth-abundant than cobalt oxides has not been reported in the photocatalytic water oxidation.

Copper complexes are attractive targets for water oxidation because of their extensive biomimetic chemistry with O_2. Although copper species have recently garnered attention for catalytic oxygen reduction, there are only two brief prior mentions of using soluble copper complexes for water oxidation, as well as a controversial report of the mechanocatalysis of water splitting by Cu_2O deposits[33]. Recently, James M. Mayer et al[34] reported copper-bipyridine complexes as water-oxidation electrocatalyst. Thomas J. Meyer et al [35]reported that simple Cu^{II} salts at a variety of electrodes are highly active in electrocatalytic water oxidation. However, the discovery of efficient water-oxidation photocatalysts based on copper metals that could be improved easily by using rational and simple synthetic schemes remain a challenge.

In this paper, we prepared $CuFe_2O_4$ nanocrystallines with cubic jacobsite structure through a facile method and firstly used it as an efficient catalyst in photocatalytic water oxidation.

It is worth noting that the $CuFe_2O_4$ catalyst exhibits excellent water oxidation capability and stability. $CuFe_2O_4$ also displays robust ferromagnetic properties, which are beneficial for easy recovery form the solution after reaction. No apparent change was shown by XPS in the surface conditions of $CuFe_2O_4$ before and after the photocatalytic reaction either.

Experimental Section

Materials

$H_2{}^{18}O$ (97% ^{18}O) was purchased from MASHALL ISOTOPES LTD. Purified water (18.2 MΩ·cm) for the preparation of solutions was obtained from a Milli Q system (Millipore, Direct-Q 3 UV), and all other chemicals and salts used were of the highest purity available from commercial sources.

Syntheses of $CuFe_2O_4$ Nanocrystallines

In a typical experiment, 8.21 g of Fe $(NO_3)_3$ $9H_2O$(0.02mol) and 1.72 g of $CuCl_2$ (0.01 mol) were dissolved in 30 mL anhydrous ethanol with continuous stirring about 30 min. Then, the 32 mL 3 mol/L of NaOH solution was added into the mixture solution formed coprecipitation product. Precipitates were collected by centrifugation and washed with deionized water and absolute ethanol for several times. Finally, the precipitates were kept at 700°C for 1 h before being naturally cooled in air.

Photocatalytic Water Oxidation.

Photocatalytic water oxidation was performed as follows. The desired concentration of catalyst 0.5 gL^{-1} was added to a buffer solution (80 mM, pH 8.5 for borate buffer) containing $[Ru(bpy)_3]$ Cl_2 (1.0 mM) and $Na_2S_2O_8$ (5.0 mM). The above solution was deaerated by purging with Ar gas for 5 min in a flask (16 mL) sealed with a rubber septum (the volume of reaction solution was 10 mL). The reaction was then started by irradiating the solution with a LED light source (light intensity 16 mW, beam diameter 2 cm) through a transmitting glass filter ($\lambda \geq 420$ nm) at room temperature. After each irradiation time, 150 μL of Ar was injected into the flask and then the same volume of gas in the headspace of the flask was withdrawn by a SGE gas-tight syringe and analysed by gas chromatography (GC). The O_2 in the sampled gas was separated by passing through a 2 m × 3 mm packed molecular sieve 5A column with an Ar carrier gas and quantified by a thermal conductivity detector (TCD) (Shimadzu GC-9A). The total amount of evolved O_2 was calculated from the concentration of O_2 in the headspace gas. Contamination of the head-space with air was corrected by measuring of N_2 present in the head-space (from the N_2 peak in the GC traces). The solution pH was measured after the reaction by a METTLER TOLEDO FEP20 pH meter.

Characterization technique

X-ray photoelectron spectra (XPS) were measured by ESCALAB250xi with X-Ray monochromatisation. GC-MS spectral analyses of isotopic labelled O_2 were performed on an Agilent Series 7890A model chromatograph interfaced with an Agilent Series 5975C model mass spectrometer. Powder X-ray diffraction (PXRD) data were collected with a PANalytical X'Pert Pro Diffractometer operated at 40 kV and 40 mA with Cu Kα radiation (step size: 0.017°, step time: 10.34 s). Field emission scanning electron microscopy (SEM) observations were performed on a Hitachi S-4800 microscope operated at an accelerating voltage of 5.0 kV. Transmission electron microscope (TEM) images were obtained with a JEOL JEM-2010 instrument operated at 200 kV.

Electrochemistry

Cyclic voltammetry (CV) was recorded on a CHI600D electrochemical analyzer, where a glassy carbon, an Ag/AgCl and a Pt wire electrodes were used as a working, reference and auxiliary electrodes, respectively. CV was obtained in buffer solutions at room temperature with a scanning rate of 100 mV s^{-1}.

Isotope-Labeled Experiment

The 10.8 atom % $H_2{}^{18}O$ of borate buffer solution (pH 8.5, 80 mM) containing $CuFe_2O_4$ (0.5 gL^{-1}), $[Ru(bpy)_3]Cl_2$ (1.0 mM), $Na_2S_2O_8$ (5.0 mM) was deaerated with Helium gas before irradiation by LED light ($\lambda \geq 420$ nm) in a flask that is sealed with a rubber septum. After 9 min, 50 μL of gas sample was withdrawn using a gas-tight syringe for gas analysis. An Agilent Series 7890A model chromatograph interfaced with an Agilent Series 5975C model mass spectrometer operating in electron impact ionization mode was used to collect mass spectrometric data. The MS detector was tuned for maximum sensitivity (quadrupole temperature, 150 °C; ion source temperature, 230 °C). Single ion mode was used to scan for the ions m/z = 28, 32, 34, 36 with a dwell time of 100 ms, resulting in 8.3 cycles per second. The ions of m/z range from 30 to 50 were also scanned in order to observe the abundance change of $^{16}O^{18}O$ and $^{18}O^{18}O$, which evolved from $H_2{}^{16}O$ and $H_2{}^{18}O$, respectively. The total flow rate into the spectrometer was limited to 0.6 mL/min. The GC equipped with a molecular sieve column (30 m × 0.32 mm × 15 μm), and the vaporizing chamber temperature and column temperature was set for 100 °C and 35 °C, respectively.

N_2 Adsorption for BET Surface Area Determination.

Nitrogen adsorption-desorption at 77 K was performed with a Micromeritics ASAP 2020M system. A sample mass of ~235 mg was used for adsorption analysis after pretreatment at 70 ℃ for ~8.0 h under vacuum conditions and kept in N_2 atmosphere until N_2-adsorption measurements. Surface areas were calculated from the adsorption data using Langmuir and Brunauer-Emmett-Teller (BET) methods.

Results and discussion

Characterization of $CuFe_2O_4$

$CuFe_2O_4$ were synthesized according to modified literature methods[36]. The size and shape of the $CuFe_2O_4$ nanoparticles obtained were investigated using TEM, as shown in Figure 1a. The particles are well dispersed with size ranging from 20 to 40 nm. To confirm the formation of $CuFe_2O_4$ crystals, nanoparticles were characterized by HRTEM as indicated in Figure 1b. The fringe spacing is about 0.162 nm, corresponding to the (321) crystal planes of $CuFe_2O_4$. The TEM and HRTEM analyses reveal that $CuFe_2O_4$ nanoparticles were polycrystalline tetragonal structure. Figure 2a shows the XRD patterns of the samples. The peak position and relative intensity of all diffraction peaks for the product match well with standard powder diffraction data. All the diffraction peaks in the XRD pattern can be indexed to those of the tetragonal structure of copper ferrite $CuFe_2O_4$ according to JCPDS file No. 34-0425. The spectrum of electron dispersive spectroscopy (EDS) (Fig. 2b) further confirms the existences of Fe, Cu, O elements in the composites. The $CuFe_2O_4$ formation proceeds may be as these: first, Cu^{2+} and Fe^{3+} ions reacted to OH^- in aqueous ethanol solution formed $Fe(OH)_3$ and $Cu(OH)_2$ coprecipitation product,

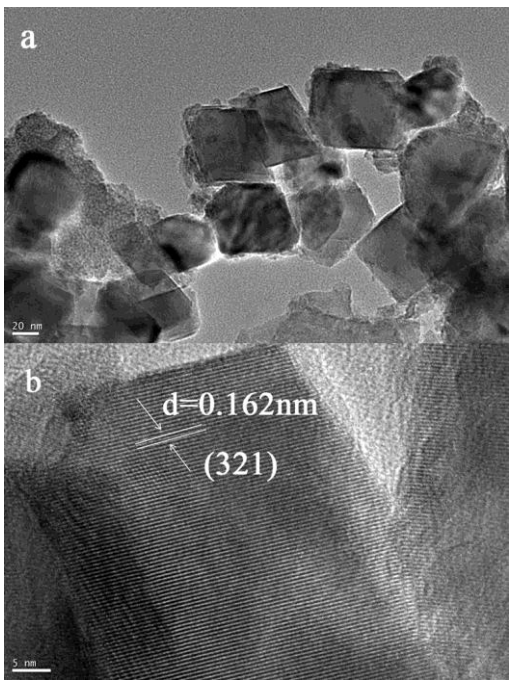

Figure 1. TEM images (a) and HRTEM (b) of $CuFe_2O_4$.

respectively (Eqs. 1 and 2). Subsequently, $CuFe_2O_4$ can be obtained from the reaction of $Fe(OH)_3$ and $Cu(OH)_2$ (Eq. 3). The chemical reaction can be expressed as follows:

$$Cu^{2+} + 2OH^- \longrightarrow Cu(OH)_2 \quad (1)$$

$$Fe^{3+} + 3OH^- \longrightarrow Fe(OH)_3 \quad (2)$$

$$Cu(OH)_2 + 2Fe(OH)_3 \xrightarrow{\triangle} CuFe_2O_4 + 4H_2O \quad (3)$$

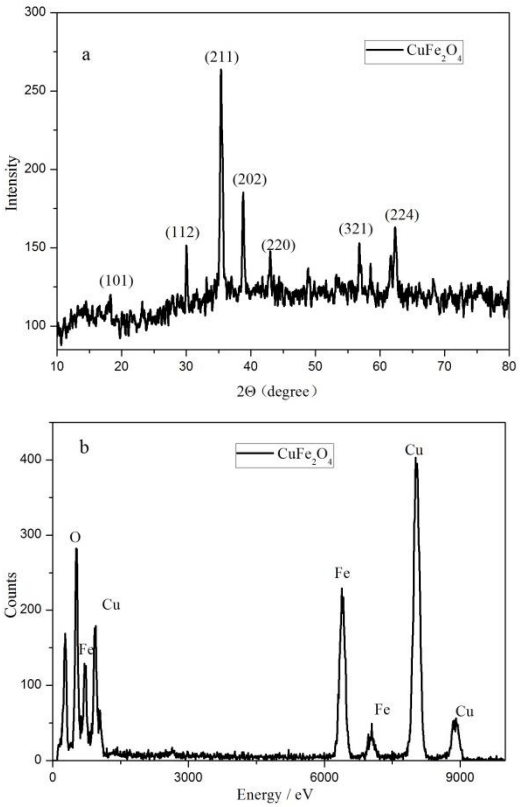

Figure 2. XRD (a) and EDS (b) of $CuFe_2O_4$.

Electrochemical properties of $CuFe_2O_4$

We further analyzed the electrochemical properties of $CuFe_2O_4$ using cyclic voltammetry. A catalytic water oxidation wave was observed at onset potential (reference

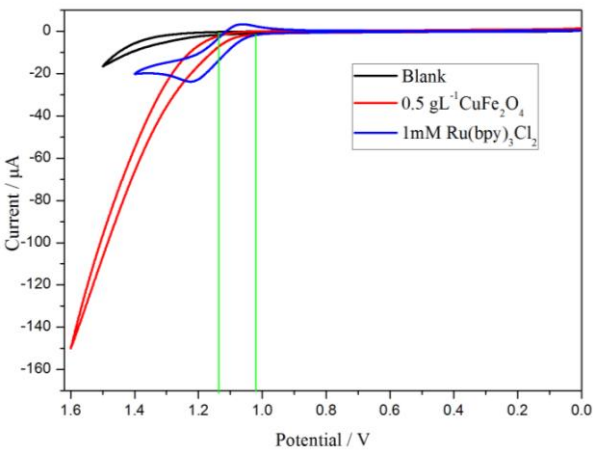

Figure 3. Cyclic voltammogram (CV) of 80 mM sodium borate buffer solution at pH 8.5 with 1.0 mM of $[Ru(bpy)_3]Cl_2$ (blue line) and $0.5gL^{-1}$ of $CuFe_2O_4$ (red line). The black line displays the CV of 80 mM sodium borate buffer solution at pH 8.5. Conditions: Cyclic voltammetry (CV) was recorded on a CHI600D electrochemical analyser with a glassy carbon pasting 0.01mg $CuFe_2O_4$, Ag/AgCl, and Pt wire electrodes as the working, reference, and auxiliary electrode, respectively, at room temperature with a scanning rate of 100 mV s^{-1}.

current value is zero)at approximately 1.02 V (vs. Ag/AgCl). In contrast, only minimum current was obtained in the same buffered solution without $CuFe_2O_4$ (Fig.3). This is clearly an indication of the ability for $CuFe_2O_4$ to catalyze the water-oxidation reaction. Moreover, the half-wave potential of $Ru(bpy)_3^{2+/3+}$ in the same buffered system are much more positive (1.13 V vs. Ag/AgCl) than the onset potential of catalytic current (1.02 V vs. Ag/AgCl) (Fig.3). Therefore, $[Ru(bpy)_3]^{3+}$ is thermodynamically capable of promoting water oxidation.

Catalytic behaviours of $CuFe_2O_4$ for photocatalytic water oxidation

Light-driven water oxidation was examined with different concentrations of $CuFe_2O_4$. Fig.4a shows that the O_2 evolution rate of all these reactions decreased over time (the slope of the kinetic curve smoothed with the lapse of time), and O_2 evolution achieved a platform in 9 min. A maximum O_2 yield (amount of O_2 produced with respect to the persulfate) of 72.8% and O_2 evolution amount of 18.2 μmol was obtained when the concentration of $CuFe_2O_4$ was 0.5 gL^{-1}. However, the catalytic activity is observed to become decreased when the concentration of $CuFe_2O_4$ was increased above 0.5 gL^{-1}.When the concentration of $CuFe_2O_4$ was increased to 1.0 gL^{-1}, the yield for O_2 evolution decreased to 62.8%. In addition, the catalytic activity is observed to become decreased when the concentration of $CuFe_2O_4$ was decreased below 0.5 gL^{-1}. When the concentration of $CuFe_2O_4$ was decreased to 0.25 gL^{-1}, the yield for O_2 evolution decreased to 52.4%. We also noticed that even under identical reaction conditions, in the absence of any catalyst, Minimum amount O_2 evolution can be detected with a value of 0.5 μmol after 9 min irradiation. In addition, no O_2 evolved when the photocatalytic water oxidation was carried out without photosensitizer or $Na_2S_2O_8$. Based on the above experimental facts and previous reports, we hypothesized that the photosensitizer can be oxidized to $[Ru(bpy)_3]^{3+}$ by $Na_2S_2O_8$ under photoirradiation, and the resulting $[Ru(bpy)_3]^{3+}$ can further oxidize water to produce O_2 thermodynamically, but with a poor selectivity and a low rate.

Water oxidation is pH-dependent and the catalytic activity of $CuFe_2O_4$ was studied under different pH conditions (Fig. 4b). The reaction at pH 8.5 showed the highest O_2 yield. The O_2 yield decreased with increasing of the pH from 8.5 to 9.0. Although a high pH is thermodynamically favourable for water oxidation, a higher pH can also accelerate the degradation of the photosensitizer, which is competitive process in the reduction of $[Ru(bpy)_3]^{3+}$ to $[Ru(bpy)_3]^{2+}$.[37-39]The buffer with pH 9.0 apparently promotes the degradation of photosensitizer under our conditions, and the original red color of the reaction solution turned much darker when the photocatalysis was carried out in the pH 9.0 buffer compared to in the pH 8.5 buffer. When the pH 8.0 buffer was used, the O_2 yield also decreased than that of the pH 8.5 buffer. A green solution was obtained after 30 s of photoirradiation of pH 8.0 buffer solution and the final pH value fell to 2.5. The solution colour

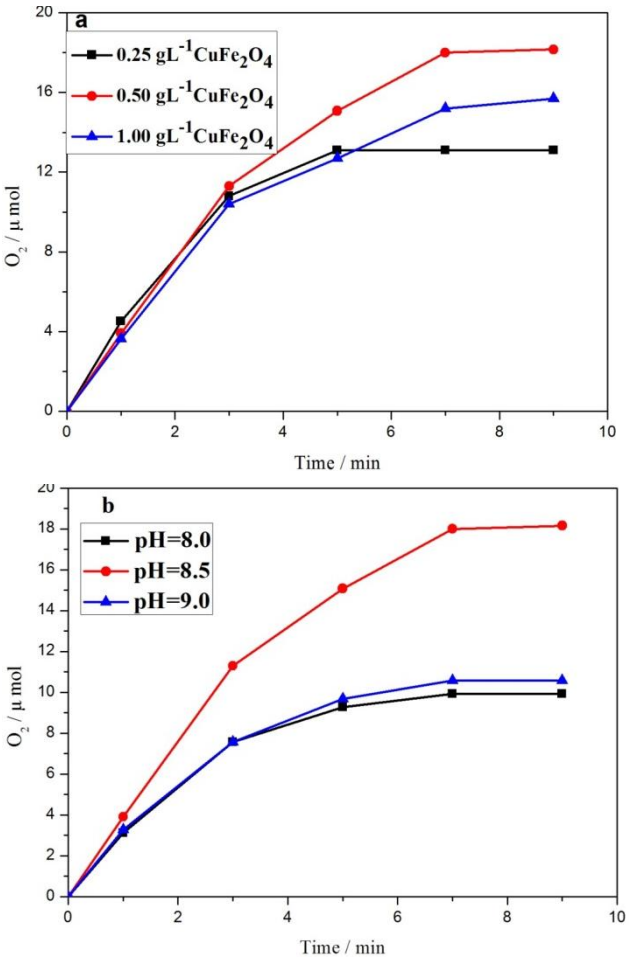

Figure 4. (a) Kinetics of O_2 formation in the photocatalytic system using different concentrations of $CuFe_2O_4$ (0.25 gL^{-1}, black; 0.5 gL^{-1}, red; 1.0 gL^{-1}, blue). Conditions: LED lamp ($\lambda \geq$ 420 nm), 1.0 mM $[Ru(bpy)_3]Cl_2$, 5.0 mM $Na_2S_2O_8$, 80 mM sodium borate buffer (initial pH 8.5), total reaction volume is 10 mL and overall volume is ~16mL, vigorous agitation using a magnetic stirrer. (b) Kinetics of O_2 formation in the photocatalytic system under various pH conditions using $CuFe_2O_4$ (pH = 8.0, 80 mM NaBi, black; pH = 8.5, 80 mM NaBi, red; pH = 9.0, 80 mM NaBi, blue). Conditions: LED lamp ($\lambda \geq$ 420 nm); catalyst concentration 0.5 gL^{-1}, 1.0 mM $[Ru(bpy)_3]$ Cl_2, 5.0 mM $Na_2S_2O_8$; total reaction volume is 10 mL and overall volume is ~16 mL; vigorous agitation using a magnetic stirrer.

became green, indicating that there was a build-up of $[Ru(bpy)_3]^{3+}$ and eqn (1) became the rate-limiting step. The presence of $[Ru(bpy)_3]^{3+}$ was proved by its characteristic absorbance at 670 nm by UV-vis (Fig. S1). The existence of build-up $[Ru(bpy)_3]^{3+}$ means that a major amount of the water oxidation oxidant could not be effectively consumed in the catalytic cycle. The pH decrease from 8.0 to 2.5 implies that the buffer capacity is deficient for maintaining the reaction pH effectively at a high and thermodynamically favourable value

for water oxidation. Moreover, the O_2 formation kinetic curve in pH 8.0 achieves a plateau in 5 minutes, which is earlier than the others, indicating that the virtual O_2 evolution time is shortened.

$$4[Ru(bpy)_3]^{3+} + 2H_2O \longrightarrow 4[Ru(bpy)_3]^{2+} + O_2 + 4H^+ \quad (4)$$

Decomposition of the photosensitizer

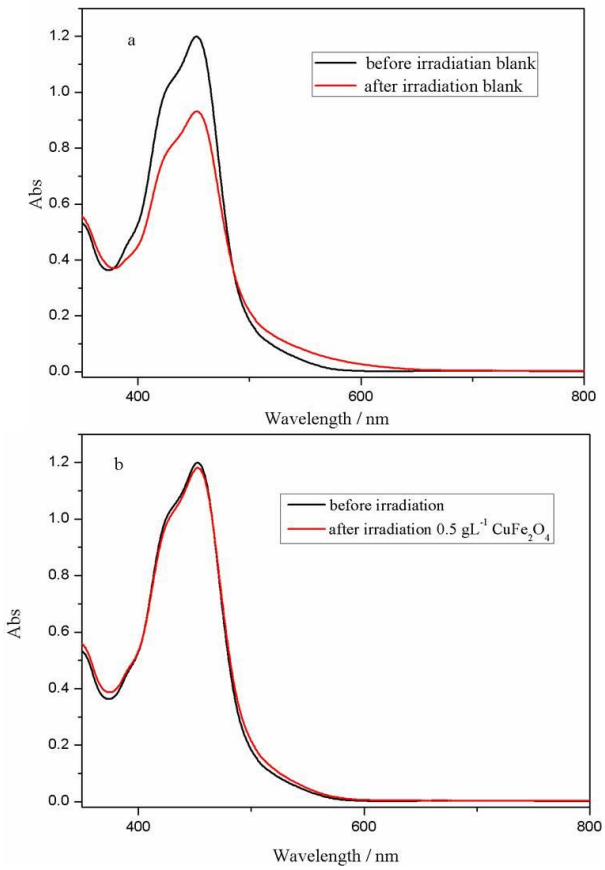

Figure 5. (a)UV-vis spectral changes during the photocatalytic O_2 evolution without any catalyst. The black line shows the absorption of aqueous borate buffer solutions (pH = 8.5, 80 mM) containing $[Ru(bpy)_3]Cl_2$ (1.0 mM) and $Na_2S_2O_8$ (5.0 mM). The red line shows the absorption of above solution after 9 min of irradiation. (b)UV-vis spectral changes during the photocatalytic O_2 evolution with $CuFe_2O_4$ .The black line shows the absorption of aqueous borate buffer solutions (pH = 8.5, 80 mM) containing $[Ru(bpy)_3]Cl_2$ (1.0 mM), $Na_2S_2O_8$ (5.0 mM) and $CuFe_2O_4$ (0.5gL^{-1}). The red line shows the absorption of above solution after 9 min of irradiation.

Self-quenching and decomposition of the photosensitizer by a nucleophilic may attack of OH^- or water on $Ru(bpy)_3^{3+}$ under neutral or basic conditions is in competition with hole transfer from $Ru(bpy)_3^{3+}$ to WOCs, leading to the decomposition of the photosensitizer and low O_2 evolution yields[38]. Thus, it is essential to find a better WOC that improves the lifetime of photosensitizer and O_2 yield consequently[37, 40, 41]. After 9 min of illumination, the concentration of $[Ru(bpy)_3]^{2+}$ decreased by 1.5% in the presence of the catalyst. Significantly, photosensitizer decomposition was markedly higher (22.4% of the initial concentration) in the absence of the catalyst, indicating that the photosensitizer is protected from decomposition in the presence of the catalyst. The UV-vis evidence supports the above argument (Fig.5).

Photocatalytic water oxidation with different metal oxides

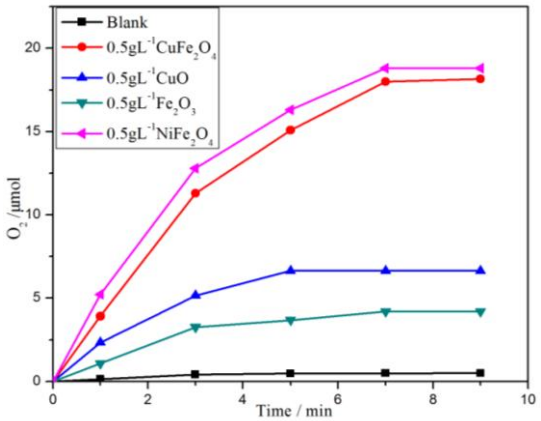

Figure6. Kinetics of O_2 formation in the photocatalytic system using different catalysts .Blank (black); Fe_2O_3 nanoparticles (green); CuO (blue); $CuFe_2O_4$ (red); $NiFe_2O_4$ (magenta).Conditions: LED lamp ($\lambda \geq 420$ nm); catalyst concentration 0.5 gL^{-1}, 1.0 mM $[Ru(bpy)_3]Cl_2$, 5.0 mM $Na_2S_2O_8$, 80 mM sodium borate buffer (initial pH 8.5); total reaction volume is 10 mL and overall volume is ~16 mL; vigorous agitation using a magnetic stirrer.

The time courses of O_2 evolution with metal oxides are shown in Fig. 6. Table 1 displays O_2 yields obtained for all of the metal oxides studied. Minimum amount of O_2 evolution was

Table 1.Water oxidation catalyzed by different catalysts.[a]

Catalyst	BET (m^2 g^{-1})	O_2(μmol)	O_2Yield (%)[b]	TOFs (μmols^{-1}m^{-2})[c]	Ref
$CuFe_2O_4$	11	18.2	72.8	1.20	this work
CuO	65	6.64	26.6	0.12	this work
Fe_2O_3	36	4.19	16.8	0.10	this work
$NiFe_2O_4$	55	18.8	75.4	0.32	this work
Fe_3O_4	45	1.50	29.0	0.04	32
$NiFe_2O_4$	48	3.70	74.0	0.11	32
$MgFe_2O_4$	-	0.95	19.0	-	32
$MnFe_2O_4$	-	0.42	8.40	-	32

[a]Conditions: LED lamp ($\lambda \geq 420$ nm); catalyst concentration 0.5 gL^{-1}, 1.0 mM $[Ru(bpy)_3]$ Cl_2, 5.0 mM $Na_2S_2O_8$, 80 mM sodium borate buffer (initial pH 8.5); total reaction volume is 10 mL and overall volume is ~16 mL; vigorous agitation using a magnetic stirrer. [b] Yield is defined as twice the number of moles of O_2 per mole of $Na_2S_2O_8$. [c] Turnover frequency normalized by a catalyst surface area for O_2 evolution in one minute.

detected in the absence of any catalysts. What is more, the amount of O_2 evolution obtained after 9 min of photoirradiation with $CuFe_2O_4$ (18.2 μmol) was larger than that with CuO (6.60 μmol) and Fe_2O_3 (4.20 μmol). Isotope-labelling water oxidation experiments demonstrate conclusively that O_2 originated from water oxidation (Fig. S2). After the 1st run of the photocatalytic reaction using simple metal oxides, Fe_2O_3 and CuO were recovered from the reaction solution for further experiment by centrifugation with a little loss. However, $CuFe_2O_4$ was collected without any loss by a magnet on account of its ferromagnetic properties (Fig. S3). A fresh buffer solution containing $Na_2S_2O_8$ (5.0 mM) and $[Ru(bpy)_3]Cl_2$ (1.0 mM) was added to the collected particles for the repetitive examinations under photoirradiation. The high catalytic activity of $CuFe_2O_4$ was maintained even after fourth and fifth runs (Fig. 7). The $CuFe_2O_4$ catalysts were examined before and after the reaction by powder XRD (Fig. 8) and TEM (Figs. S4-5) measurements.

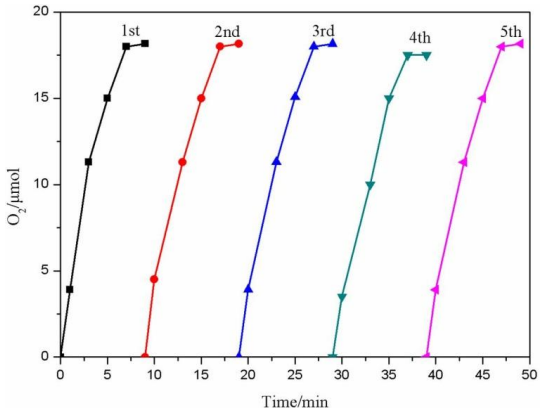

Figure 7. Kinetics of O_2 formation in the photocatalytic system using fresh $CuFe_2O_4$ and recovered $CuFe_2O_4$. first run (black); second run (red); third run (blue); fourth run (green); fifth run (magenta).Conditions: LED lamp ($\lambda \geq 420$ nm); catalyst concentration 0.5 gL^{-1}, 1.0 mM $[Ru(bpy)_3]Cl_2$, 5.0 mM $Na_2S_2O_8$, 80 mM sodium borate buffer (initial pH 8.5); total reaction volume is 10 mL and overall volume is ~16 mL; vigorous agitation using a magnetic stirrer.

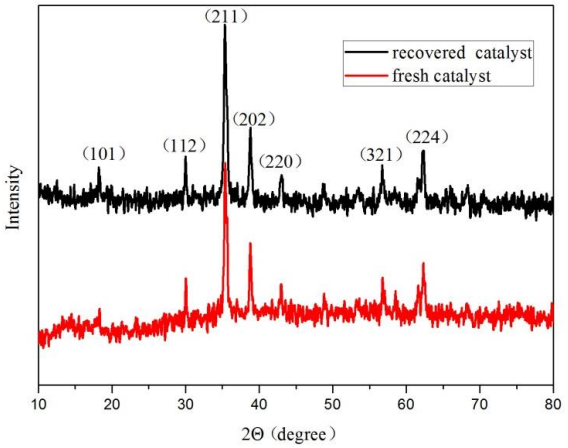

Figure8. XRD of fresh $CuFe_2O_4$ (red) and recovered $CuFe_2O_4$ (black).

No obvious variation in either powder XRD pattern or the morphology of the $CuFe_2O_4$ catalysts was observed. These results clearly indicate that $CuFe_2O_4$ is a highly active and robust catalyst in the photocatalytic system.

According to the previous work[32], the amount of O_2 evolution (3.7 μmol) from the reaction solution with $NiFe_2O_4$ was higher than that with Fe_3O_4 (1.5 μmol). Incorporation Ni^{2+} enhances the water oxidation reactivity of iron oxides as the case of the visible light-driven catalytic water oxidation. While the amounts of evolved O_2 from reaction solutions with $MgFe_2O_4$ (0.95 μmol) and $MnFe_2O_4$ (0.42 μmol) were smaller than that with Fe_3O_4 (1.5 μmol).These results suggest not all the foreign metal ion doping of iron oxides enhances the water oxidation reactivity of iron oxides. Catalytic activity of CuO for the photocatalytic water oxidation has been examined, however, the amount of O_2 evolution was around 6.6 μmol, which is only one third of that with $CuFe_2O_4$.The O_2 yield with $CuFe_2O_4$ (72.8%, pH 8.5) is comparable to that of catalysts with $NiFe_2O_4$ particles (75.4%, pH 8.5). The catalytic activities of heterogeneous catalysts are usually investigated on the basis of normalization by the specific surface area. So, in order to obtain the apparent turnover frequencies (TOFs), rate of oxygen evolution (R_{O2}) values calculated from the initial slope (1 min) of time courses were divided by the BET surface areas through N_2 adsorption measurements at 77 K (11 m^2g^{-1} for $CuFe_2O_4$). The apparent TOF value of 1.2 $\mu mols^{-1}m^{-2}$ was obtained with $CuFe_2O_4$. Moreover, in our work, despite the smaller specific surface area of $CuFe_2O_4$ (11 m^2g^{-1}) than $NiFe_2O_4$ nanoparticles (55 m^2g^{-1}), the apparent TOF value of $CuFe_2O_4$ (1.2 $\mu mols^{-1}m^{-2}$) was larger than that of $NiFe_2O_4$ nanoparticles (0.32 $\mu mols^{-1}m^{-2}$). These results clearly indicate that Cu atom of $CuFe_2O_4$ is a highly active O_2- evolving sites. Moreover, subunit structure of spinel $CuFe_2O_4$ (Fig.9b) may provide a new experimental basis for modelling PSII-inspired water oxidation mechanisms.

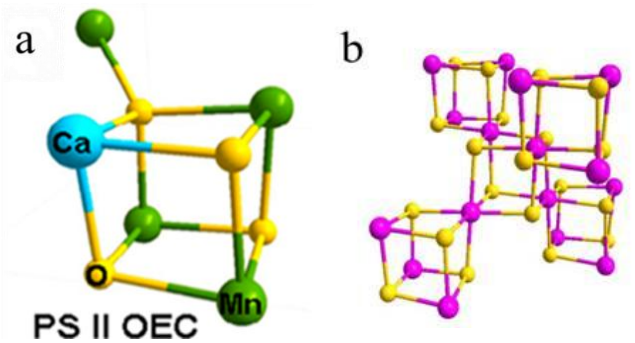

Figure 9. Crystal structures of active water oxidation catalysts: (a) PSII-WOC; (b) spinel $CuFe_2O_4$ subunit structure. :O :Fe/Cu. (The chances of distributing iron and copper in the same position are equal and it is difficult to differentiate iron and copper.)

In this report, the high O_2 yield with $CuFe_2O_4$ is attributed to the synergetic effect that stems from the unique $CuFe_2O_4$ nanostructures consisting of two different O_2-evolving sites. The $CuFe_2O_4$ should provide a facile hole pathway from photo-

generated $Ru(bpy)_3^{3+}$ molecules[42] (Fig. S6) to the Cu atoms and Fe atoms which are O_2-evolving sites in the nanostructures.

To our knowledge, Co_3O_4 possessed high catalytic activity in the photocatalytic water oxidations. The apparent TOF value with $CuFe_2O_4$ is larger than that with Co_3O_4 (0.14 $\mu mols^{-1}m^{-2}$)[32]. The O_2 yield with $CuFe_2O_4$ (72.8%, pH 8.5) is also higher than those reported with catalysts containing precious metals like RuO_2 particles (22%, pH 5.0)[9], IrO_2 particles (69%, pH 5.0)[9] and abundant elements such as Fe_2O_3 particles (16.8%, pH 8.5), CuO particles (26.6%, pH 8.5) and Mn_xO_y particles (55%, pH 5.8)[43]. These results indicate that the high activity of $CuFe_2O_4$ results from the composite effect of copper and iron oxides. At the same time, the O_2 yield is comparable to that of catalysts with abundant metals, for example, $LaCoO_3$ particles (74%, pH 7.0)[31]. Hence, $CuFe_2O_4$ composed of earth-abundant elements turns out to be one of the most active catalysts for photocatalytic water oxidation.

Study of surface conditions for recovered $CuFe_2O_4$

A critical issue of some spinel compounds is that their divalent metal species can be oxidized under highly oxidizing conditions, which may result in micro-phase separation and deactivation of the catalysts. Therefore, it is of great necessity to confirm the surface conditions of each component after water oxidation. A series of measurements were taken based on the knowledge above. The change of the surface conditions of $CuFe_2O_4$ before and after the photocatalytic reaction was observed by XPS. The XPS measurements were performed for the energy regions of full scan, Fe 2p, Cu 2p and O 1s energy regions. The binding energy of each element was corrected by C 1s peak (284.8 eV). Fig.10a displays the XPS spectra of Fe $2p_{3/2}$ peak at 709.6 eV with a weak satellite peak at 718.3 eV and Fe $2p_{1/2}$ peak at 722.8 eV for $CuFe_2O_4$ before the reaction. A Fe $2p_{3/2}$ peak at 709.7 eV with a weak satellite peak at 718.4 eV and a Fe $2p_{1/2}$ peak at 722.8 eV after the reaction are also shown in Fig.10a. These peaks are assigned to Fe^{3+} by comparison with the Fe 2p peaks of Fe_2O_3[44]. The similar ratios of peak strength between Fe 2p main peak and satellite peak for both samples support that the surface conditions remain unchanged even after the photocatalytic water oxidation under highly oxidizing conditions. Fig. 10b shows the XPS spectra for Cu $2p_{3/2}$ peaks and Cu $2p_{1/2}$ peaks appear at 932.0 eV and 951.9 eV with weak satellite peaks for $CuFe_2O_4$ samples before and after the reaction. The binding energies of these peaks indicate the Cu species in the samples are Cu^{2+} by comparison with peak positions of Cu 2p peaks of CuO peaks[45]. Fig. 10c exhibits the XPS spectra for O 1s peak appeared 528.6 eV with an another peak at 530.2 eV for $CuFe_2O_4$ before the reaction and that at 528.7 eV with an another peak at 530.3 eV after the reaction. Although the main peak of Fe 2p and O 1s from the sample after the reaction slightly shifted in the direction of higher binding energy region, the identical separation between main peak and satellite peak in both samples and consistency of peak shapes, clearly illustrate that there were no change in the valence state of Cu^{2+}, $Fe^{3+}$and O^{2-}. Thus, $CuFe_2O_4$ is highly robust even during the photocatalytic water oxidation. On the other hand, the intensity of Cu2p peaks is indeed less intense after photocatalysis and the O1s signals have different intensities after the photocatalysis. The XPS measurements indicate the following points: (i) on a qualitative basis the absence of additional peaks and/or peak shifts after photocatalysis clearly supports the absence of surface modifications, (ii) on a quantitative basis the decrease of Cu2p and O1s (the one at 530 eV) peak intensities is consistent with partial Cu^{2+} loss.

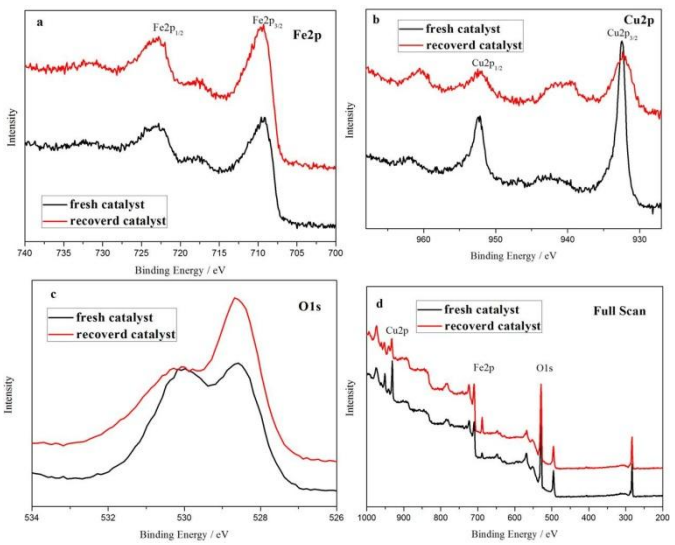

Figure 10. X-ray photoelectron spectra of $CuFe_2O_4$ before and after the reaction in the energy regions of (a) Fe 2p, (b) Cu 2p, (c) O 1s and (d) full scan of $CuFe_2O_4$ before and after the reaction.

Mechanism study

The reaction was performed by the photoirradiation ($\lambda \geq 420$ nm) of a borate buffer (80 mM, pH 8.5, 10 mL) containing a metal oxide catalyst, $Na_2S_2O_8$ as the sacrificial electron acceptor, and $[Ru(bpy)_3]$ Cl_2 as the photosensitizer. The catalytic cycle of the visible light-driven water oxidation is depicted in Scheme 1. In the $Ru(bpy)_3^{2+}$–$S_2O_8^{2-}$ method, the sensitizer of $Ru(bpy)_3Cl_2$ absorbs visible light and gives electrons to the sacrificial electron acceptor $S_2O_8^{2-}$, then, which is reduced to SO_4^{2-}. $Ru(bpy)_3^{2+}$ transforms into $Ru(bpy)_3^{2+*}$ (where the * denotes the excited state) because of photo induction, then $Ru(bpy)_3^{2+*}$ transfers electron to $S_2O_8^{2-}$, producing $Ru(bpy)_3^{3+}$, SO_4^{2-} and $SO_4^{\cdot-}$. $SO_4^{\cdot-}$ {$[E^0(SO_4^{\cdot-}/SO_4^{2-})$ = +2.40 V vs. Ag/AgCl]}[31], whose electrode potential is higher than that of {$[E^0(Ru(bpy)_3^{2+}/Ru(bpy)_3^{3+})$= +1.22 V vs. Ag/AgCl]}[46, 47], can oxide another $Ru(bpy)_3^{2+}$ to produce two

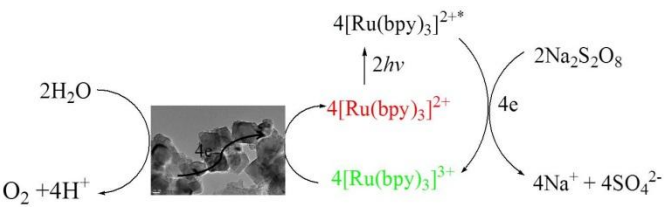

Scheme 1. Principal Processes of O_2 Evolution Light-Driven Water Oxidation System

equiv. of $Ru(bpy)_3^{3+}$ in the overall photoinduced process. Finally, $Ru(bpy)_3^{3+}$ pulls four electrons sequentially from the catalyst and two water molecules are oxidized to form one oxygen molecule (Scheme 1).

Conclusions

In summary, $CuFe_2O_4$ nanocrystallines with cubic jacobsite structure have been obtained. Disclosed here is the first example of a copper-based photocatalyst for water oxidation. As is expected, the $CuFe_2O_4$ show convenience for separation and durable excellent water oxidation activity, as evidenced by the maintenance of a high O_2 yield after 5 repeated uses. Slightly absence was shown by XPS in the surface conditions of $CuFe_2O_4$ before and after the photocatalytic reaction either. Subunit structure of spinel $CuFe_2O_4$ may provide a new experimental basis for modelling PSII-inspired water oxidation mechanisms. Copper-based catalysts described herein clearly fill a gap in the design of water-splitting systems, which could eventually enable for sustainable artificial photosynthetic schemes.

Acknowledgements

This work was financially supported by the National Natural Science Foundation of China (Grant Nos. 21173105, 21376020), the Fundamental Research Funds for the Central Universities (lzujbky-2014-67) and State Key Laboratory of Chemical Resource Engineering Beijing University of Chemical Technology.

Notes and references

[a] Key Laboratory of Nonferrous Metal Chemistry and Resources Utilization of Gansu Province, College of Chemistry and Chemical Engineering, Lanzhou University, Lanzhou 730000, China

[b] State Key Laboratory of Chemical Resource Engineering, Beijing University of Chemical Technology

Email:dingyong1@lzu.edu.cn

† Electronic Supplementary Information (ESI) available: [details of any supplementary information available should be included here]. See DOI: 10.1039/b000000x/

1. M. W. Kanan and D. G. Nocera, *Science*, 2008, **321**, 1072-1075.
2. F. Evangelisti, R. Guttinger, R. More, S. Luber and G. R. Patzke, *J. Am. Chem. Soc.*, 2013, **135**, 18734-18737.
3. T. Nakagawa, N. S. Bjorge and R. W. Murray, *J. Am. Chem. Soc.*, 2009, **131**, 15578-15579.
4. R. Cao, H. Ma, Y. V. Geletii, K. I. Hardcastle and C. L. Hill, *Inorg. Chem.*, 2009, **48**, 5596-5598.
5. J. F. Hull, D. Balcells, J. D. Blakemore, C. D. Incarvito, O. Eisenstein, G. W. Brudvig and R. H. Crabtree, *J. Am. Chem. Soc.*, 2009, **131**, 8730-8731.
6. L. Duan, F. Bozoglian, S. Mandal, B. Stewart, T. Privalov, A. Llobet and L. Sun, *Nat. Chem.*, 2012, **4**, 418-423.
7. L. Duan, A. Fischer, Y. Xu and L. Sun, *J. Am. Chem. Soc.*, 2009, **131**, 10397-10399.
8. Y. V. Geletii, B. Botar, P. Kogerler, D. A. Hillesheim, D. G. Musaev and C. L. Hill, *Angew. Chem., Int. Ed.*, 2008, **47**, 3896-3899.
9. A. Harriman, I. J. Pickering, J. M. Thomas and P. A. Christensen, *J. Chem.Soc., Faraday Trans.1*, 1988, **84**, 2795-2806.
10. F. Jiao and H. Frei, *Energy Environ. Sci.*, 2010, **3**, 1018-1027.
11. S. Fukuzumi, D. Hong and Y. Yamada, *J. Phys. Chem. Lett.*, 2013, **4**, 3458-3467.
12. M. P. Santoni, G. La Ganga, V. Mollica Nardo, M. Natali, F. Puntoriero, F. Scandola and S. Campagna, *J. Am. Chem. Soc.*, 2014, **136**, 8189-8192.
13. X. Du, J. Wei, J. Zhao, R. Han and Y. Ding, *Chem. Asian. J.*, 2014, **9**, 2745-2750.
14. A. Indra, P. W. Menezes, N. R. Sahraie, A. Bergmann, C. Das, M. Tallarida, D. Schmeisser, P. Strasser and M. Driess, *J. Am. Chem. Soc.*, 2014, **136**, 17530-17536.
15. F. Yu, F. Li, B. Zhang, H. Li and L. Sun, *ACS Catal.*, 2015, **5**, 627-630.
16. S. Fu, Y. Liu, Y. Ding, X. Du, F. Song, R. Xiang and B. Ma, *Chem. Commun.*, 2014, **50**, 2167-2169.
17. C. Leung, S. Ng, C. Ko, W. Man, J. Wu, L. Chen and T. Lau, *Energy Environ. Sci.*, 2012, **5**, 7903-7907.
18. J. L. Fillol, Z. Codolà, I. Garcia-Bosch, L. Gómez, J. J. Pla and M. Costas, *Nat. Chem.*, 2011, **3**, 807-813.
19. M. Zhang, M. T. Zhang, C. Hou, Z. F. Ke and T. B. Lu, *Angew. Chem. Int. Ed.*, 2014, **53**, 13042-13048.
20. C. Panda, J. Debgupta, D. Diaz Diaz, K. K. Singh, S. Sen Gupta and B. B. Dhar, *J. Am. Chem. Soc.*, 2014, **136**, 12273-12282.
21. T. Zhang, C. Wang, S. Liu, J. L. Wang and W. Lin, *J. Am. Chem. Soc.*, 2014, **136**, 273-281.
22. N. S. McCool, D. M. Robinson, J. E. Sheats and G. C. Dismukes, *J. Am. Chem. Soc.*, 2011, **133**, 11446-11449.
23. A. M. Ullman, Y. Liu, M. Huynh, D. K. Bediako, H. Wang, B. L. Anderson, D. C. Powers, J. J. Breen, H. D. Abruna and D. G. Nocera, *J. Am. Chem. Soc.*, 2014, **136**, 17681-17688.
24. H. Lv, J. Song, Y. V. Geletii, J. W. Vickers, J. M. Sumliner, D. G. Musaev, P. Kogerler, P. F. Zhuk, J. Bacsa, G. Zhu and C. L. Hill, *J. Am. Chem. Soc.*, 2014, **136**, 9268-9271.
25. X. B. Han, Z. M. Zhang, T. Zhang, Y. G. Li, W. Lin, W. You, Z. M. Su and E. B. Wang, *J. Am. Chem. Soc.*, 2014, **136**, 5359-5366.
26. F. Song, Y. Ding, B. Ma, C. Wang, Q. Wang, X. Du, S. Fu and J. Song, *Energy Environ. Sci.*, 2013, **6**, 1170–1184.
27. Q. Yin, J. M. Tan, C. Besson, Y. V. Geletii, D. G. Musaev, A. E. Kuznetsov, Z. Luo, K. I. Hardcastle and C. L. Hill, *Science*, 2010, **328**, 342-345.
28. F. Song, Y. Ding and C. Zhao, *Acta Chim. Sinica*, 2014, **72**, 133-144.
29. P. Car, M. Guttentag, K. K. Baldridge, R. Alberto and G. R. Patzke, *Green Chem.*, 2012, **14**, 1680-1688.
30. G. Chen, L. Chen, S. M. Ng and T. C. Lau, *ChemSusChem*, 2014, **7**, 127-134.
31. Y. Yamada, K. Yano, D. Hong and S. Fukuzumi, *Phys. Chem. Chem. Phys.*, 2012, **14**, 5753-5760.
32. D. Hong, Y. Yamada, T. Nagatomi, Y. Takai and S. Fukuzumi, *J.Am.Chem.Soc.*, 2012, **134**, 19572-19575.
33. P. E. de Jongh, D. Vanmaekelbergh and J. J. Kelly, *Chem. Commun.*, 1999, 1069-1070.
34. Shoshanna M. Barnett, K. I. Goldberg and J. M. Mayer, *Nat. Chem.*, 2012, **4**, 498-502.
35. Z. Chen and T. J. Meyer, *Angew. Chem. Int. Ed.* , 2013, **52**, 700-703.

36. H. Jiao, G. Jiao and J. Wang, *Synthesis and Reactivity in Inorganic, Metal-Organic, and Nano-Metal Chemistry*, 2013, **43**, 131-134.
37. D. Hong, J. Jung, J. Park, Y. Yamada, T. Suenobu, Y.-M. Lee, W. Nam and S. Fukuzumi, *Energy Environ.Sci.*, 2012, **5**, 7606-7616.
38. C. Creutz and N. Sutin, *Proc. Natl. Acad. Sci. U.S.A.*, 1975, **72**, 2858-2862.
39. P. K. Ghosh, B. S. Brunschwig, M. Chou, C. Creutz and N. Sutin, *J. Am. Chem. Soc.*, 1984, **106**, 4772-4783.
40. N. D. Morris and T. E. Mallouk, *J. Am. Chem. Soc.*, 2002, **124**, 11114-11121.
41. D. Hong, Y. Yamada, A. Nomura and S. Fukuzumi, *Phys. Chem. Chem. Phys.*, 2013, **15**, 19125-19128.
42. M. Natali, S. Berardi, A. Sartorel, M. Bonchio, S. Campagna and F. Scandola, *Chem. Commun.*, 2012, **48**, 8808-8810.
43. F. Jiao and H. Frei, *Chem. Commun.*, 2010, **46**, 2920-2922.
44. M. Descostes, F. Mercier, N. Thromat, C. Beaucaire and S. M. Gautier *Appl. Surf. Sci.*, 2000, **165**, 288.
45. Lj. Kundakovic and M. F. Stephanopoulos, *Appl. Catal. A*, 1998, **171**, 13-29.
46. C. Creutz and N. Sutin, *Inorg. Chem.*, 1976, **15**, 496-499.
47. H. Lv, J. Song, H. Zhu, Y. V. Geletii, J. Bacsa, C. Zhao, T. Lian, D. G. Musaev and C. L. Hill, *J. Catal.*, 2013, **307**, 48-54.